J Nanostruct 13(4): 948-959, Autumn 2023

RESEARCH PAPER

Synthesis and Investigation of $CuFe_2O_4$-Al_2O_3 Magnetic Nanocomposite in Order to Remove Methyl Red and Methyl Orange Toxic Pollutants from Aqueous Solutions

Sohrab Kahrizi Baaghmoori [1], *and Farnaz Maghazeii* [2] *

[1] *Master of Science Student in Nano Physics, Arak Branch, Islamic Azad University, Arak, Iran*

[2] *Mathematics and Physics Department, Science Faculty, Arak Branch, Islamic Azad University, Arak, Iran*

ARTICLE INFO

Article History:
Received 02 June 2023
Accepted 21 September 2023
Published 01 October 2023

Keywords:
Magnetic nanoparticles
Nanocomposite
Photocatalytic behavior
Toxic dyes

ABSTRACT

In this research, magnetic and photocatalytic nanoparticles of copper ferrite were synthesized using hydrothermal methods. The synthesis was repeated in the presence of ultrasound waves to determine the effect of these waves on the nanostructure of the materials. photocatalytic property of copper ferrite was investigated in the degradation of two toxic dyes, methyl orange and methyl red under UV- IR radiation. Due to magnetic property of copper ferrite nanoparticles, they have the ability to direct photocatalytic reaction products out of the reaction environment too. On the other hand, aluminum hydroxide and aluminum oxide nanoparticles were also synthesized by the same method. Aluminum oxide nanoparticles with high porosity are very suitable absorbents for color absorption. Finally, a core-shell magnetic nanocomposite was made with copper ferrite, alumina and aluminum hydroxide absorbers with hydrothermal method assisted by ultrasound waves and the photocatalytic potential of prepared nanocomposite was assessed using acidic pH methyl orange and methyl red solutions under UV- IR radiation. Also all of products were analyzed by X-ray diffraction (XRD), scanning electron microscope (SEM) and vibrating sample magnetometry (VSM).

How to cite this article
Kahrizi Baaghmoori S, Maghazeii F. Synthesis and Investigation of $CuFe_2O_4$-Al_2O_3 Magnetic Nanocomposite in Order to Remove Methyl Red and Methyl Orange Toxic Pollutants from Aqueous Solutions. J Nanostruct, 2023; 13(4):948-959. DOI: 10.22052/JNS.2023.04.005

INTRODUCTION

Metals and metal oxides, commonly known as magnetic materials such as iron, cobalt, nickel, copper and … are widely used in industry. These materials react to an external magnetic field and deviate in its presence. Conductivity, mechanical strength and other magnetic properties of magnetic particles increase greatly as their dimensions decrease to nanometers. In fact, magnetic materials in very small dimensions have different properties compared to the large volume of that material.

Magnetic nanoparticles, which are usually ferromagnetic, lose their magnetic properties at a temperature higher than a certain limit. The temperature at which permanent magnetism will change to induction magnetism and vice versa is called Curie temperature. The magnetic behavior of various compounds is divided into five main categories based on how they respond to an applied external field: dia-magnetism, para-magnetism, ferro-magnetism, ferri-magnetism

* *Corresponding Author Email: fmaghazeii@iau.ac.ir*

and anti-ferromagnetism [1-5].

Copper ferrite (CuFe2O4: including spinel ferrites and soft magnetic materials) is one of the most important magnetic materials, because it has interesting electrical and magnetic properties with thermal and chemical stability and is widely used in the electronics industry. Copper ferrite is a valuable spinel ferrite because of its ability to change its physical properties such as phase transition, electrical switching, semiconductor, magnetic, and electrical properties. Also, the ability to precisely adjust the structural morphology, it makes copper ferrite an important ferrite. Copper ferrite nanoparticles are usually small in size and have a higher surface-to-volume ratio and may accumulate when dispersed in water. Therefore, partial or complete coating of these nanoparticles helps to improve their stability in facing different environments [6-9].

A photocatalyst is defined as a compound or a substance which is capable to produce chemical transformations of the reaction partners upon absorption of light. The excited state of the photocatalyst repeatedly interacts with the reaction partners forming reaction intermediates and remain intact or regenerates itself after each cycle of such interactions [10,11]. Light absorption by photocatalysts (usually UV radiation) results an excitation in valence band electrons, therefore moving them into conducting band. These electrons have reduction activity. The remaining holes in valence band possess powerful oxidation property. Electron-hole pairs react with pollutants on the surface of catalyst particles and converting them into simpler and far less dangerous materials [12,13] therefore, the separation of produced electrons and holes shows the efficiency of the photocatalysis phenomena [14-18]. The synthesis of photocatalysts in nano scale with high surface/ volume ratio increases surface absorption and improves photocatalytic property [11,19]. Metal oxides including Al_2O_3 as nanoscale absorbers have long been of interest to researchers. Research has shown that Al_2O_3 has very good surface absorption in terms of capacity and selectivity for metal pollution and other common pollution such as water-soluble azo dyes. Al_2O_3 or aluminum dioxide is one of the most widely used aluminum oxides and is specifically introduced as aluminum oxide, which is usually called alumina. Gamma alumina is most widely used in the catalyst industry due to its high surface area. Aluminum oxide is an electrical insulator, but it also has high thermal conductivity. Although this thermal conductivity changes with temperature. This material also has a high melting point [20-26].

In our research, at first we synthesized copper ferrite and alumina nanoparticles using hydrothermal method once in the presence of ultrasound waves and again without using these waves. In second step, Al_2O_3/$CuFe_2O_4$ core-shell magnetic nanocomposite was prepared using hydrothermal method assisted by ultrasound waves. XRD, SEM and VSM analysis for the samples were done. Finally, the photocatalytic behavior of synthetic nanocomposite for degradation of methyl orange and methyl red toxic dyes via UV-visible light irradiation was studied.

MATERIALS AND METHODS

Materials and devices

We used $CuCl_2.2H_2O$, $Fe(NO_3)_3$, NaOH, $Al(NO_3)_3$ from Merck company and distilled water and hydrochloric acid as raw materials for preparing of our nanomaterials.

Nanoparticles were synthesized by ultrasonic method. Ultrasound devices was FAPN400.

To determine the structural characterization of samples, we used XRD analysis with CuKα (λ = 1.5418 Å) in the range of 2θ= 10-80° . SEM images were obtained by MIRA3 TESCAN SEM.

Magnetic properties were evaluated using a VSM at room temperature (Magnetic Daghigh Daneshpajouh Co., Iran) in an applied magnetic field sweeping between ±10000Oe.

Copper ferrite synthesis method

0.5 g $CuCl_2.2H_2O$ and 2.36 g $Fe(NO_3)_3$ (molar ratio 1:2) were dissolved in 150 ml distilled water and was stirred by a magnetic stirrer. The measured pH of the solution was 3. The same amount of iron salt was again dissolved in 50 ml distilled water as before and then added to the original solution drop by drop and each time the acidity of the solution was checked by litmus paper. By adding 2 ml of iron salt solution to the initial solution, the pH of solution reached 2 and by pouring 50 ml completely on the initial 150 ml, the pH value of the solution reached 1. Then the solution was put on the stirrer and NaOH solution (1M) was slowly added to it until its pH reach 11. In this stage, the solution was put in the ultrasonic device with a power of 50% and 400 watts at room temperature and the addition of NaOH was continued until

the color of it becomes cloudy. Then the power of the device was changed to 25% and about 30 ml of NaOH was again added to the solution until the color of it turned dark blue. This solution was placed in the ultrasonic device for another 30 minutes, and then was poured into two test tubes and placed in the reactor at 240°C for 5 hours and then was left in the furnace for 24 hours until becomes clear and the sediment settles. Materials in both test tubes were centrifuged several times after cooling and we washed them thrice with de-ionized water. The products dried in oven at 50°C for 48 hours to get the desired powder from each one.

The synthesis of $CuFe_2O_4$ was repeated exactly once without the presence of ultrasound waves.

Alumina synthesis method

1 g of aluminum nitrate ($Al(NO_3)_3$) was dissolved in 200ml of distilled water and place a magnet inside it and was stirred by magnetic stirrer at room temperature for about 10 minutes to produce a clear solution. NaOH solution (1M) was slowly added to solution as a precipitating agent and the acidity of the solution was checked by litmus paper. pH of solution was adjusted at 11 which measured by calibrated pH meter. Then we removed the magnet from the solution and poured it in the flask and put the flask inside the autoclave reactor at 240 °C for 5 hours. The synthesized material was centrifuged after cooling. A white sediment remains at the end of test tube, which was thought to be $Al(OH)_3$. Finally, the obtained solution is centrifuged, washed with distilled water and alcohol and dried in the oven. We heat it at the temperature of 50 °C in the oven (in the crucible so that it does not break) for 24 hours to turn into Al_2O_3. To convert into Al_2O_3 phase, we expected that calcination at temperatures above 400^{0}C would be required. But XRD pattern of the sample shows that pure phase aluminum oxide was synthesized only by using hydrothermal at the specified temperature, fortunately. Due to the presence of pressure in the autoclave reactor, the hydroxide phase has the ability to transform $Al(OH)_3$ into Al_2O_3.

Alumina synthesis was repeated once again, but this time the sample was placed in ultrasonic device with a power of 400 W for 30 minutes before being placed in the autoclave reactor.

Synthesis of Al_2O_3 /$CuFe_2O_4$ nanocomposite with hydrothermal method assisted by ultrasound waves

Synthesized alumina was used for preparing of our nanocomposite but, in order for the alumina to contain a layer of $Al(OH)_3$, the calcination was performed at 400 °C for 2 hours. Aluminum hydroxide is very hydrophobic due to the abundant hydroxides on its structure, and therefore was used for making our composite. The Al_2O_3 sample after cooling was poured into 200 ml of distilled water with molar ratio of 1:1 and the result solution was placed in the ultrasonic device until Al_2O_3 was completely spread in the distilled water under ultrasound waves.

In the next step, 0.5 g copper salt ($CuCl_2$) and 2.36 g iron salt ($Fe(NO_3)_3$) were added to the solution and stirred with magnetic stirrer. Then, NaOH solution (1M) was slowly added to the solution until its color changed to brown and sediment settled (about 11 ml). Beaker containing

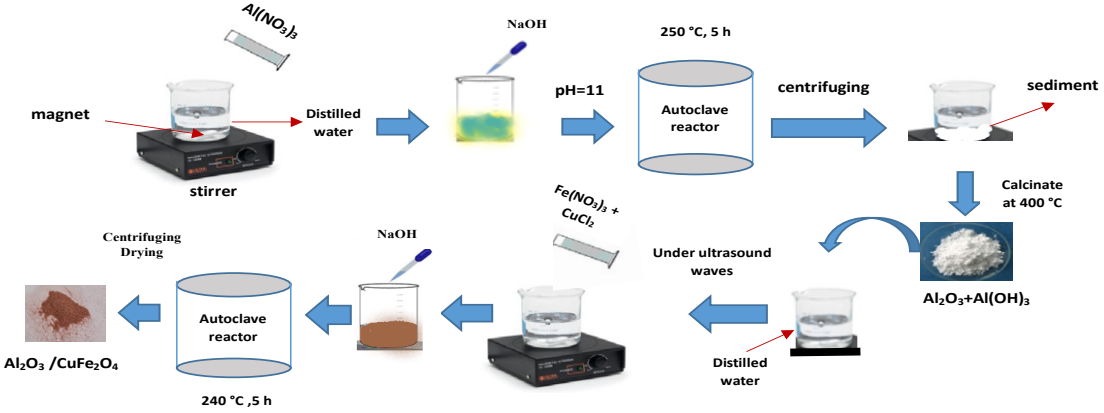

Fig. 1. Schematic diagram for Al_2O_3/$CuFe_2O_4$ nanocomposite synthesis

the solution was placed in the autoclave reactor for 5 hours at a temperature of 240°C. The synthesized material was centrifuged after cooling and its excess water was poured out and put in the oven for 24 hours at 50°C for completely drying (Fig. 1).

RESULTS AND DISCUSSION

Fig. 2 shows XRD pattern of copper ferrite nanoparticles. The XRD pattern reveals the typical diffraction pattern of pure cubic phase which is consistent of pure phase of $CuFe_2O_4$ in agreement with JCPDS 77-0010. XRD pattern of Al_2O_3 nanoparticles is illustrated in Fig. 3. Most of the observed peaks in the pattern are in agreement with standard peaks of rhombohedral phase with JCPDS 42-1468, also there are some peaks related to tetragonal phase in agreement with JCPDS 47-

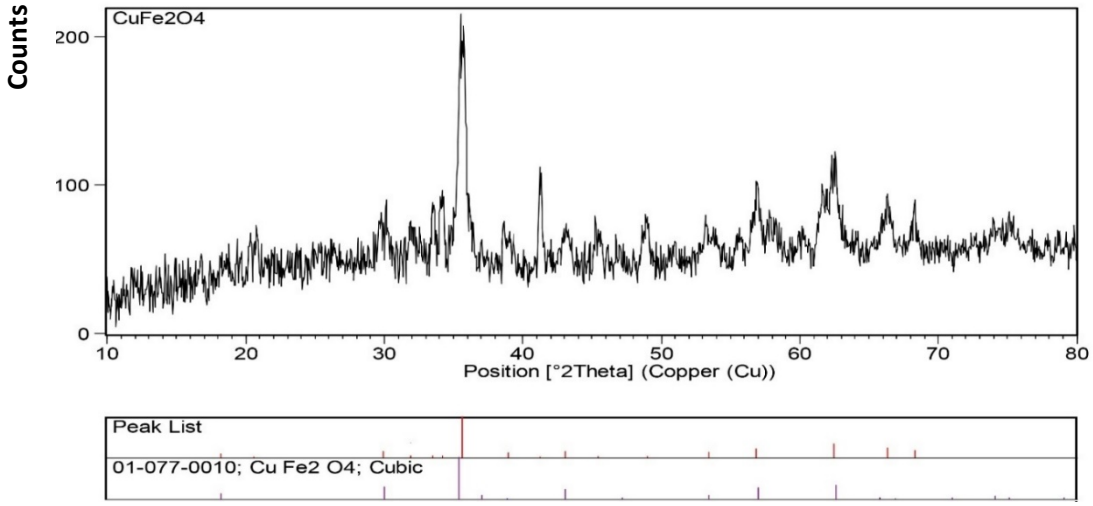

Fig. 2. XRD pattern of copper ferrite nanoparticles

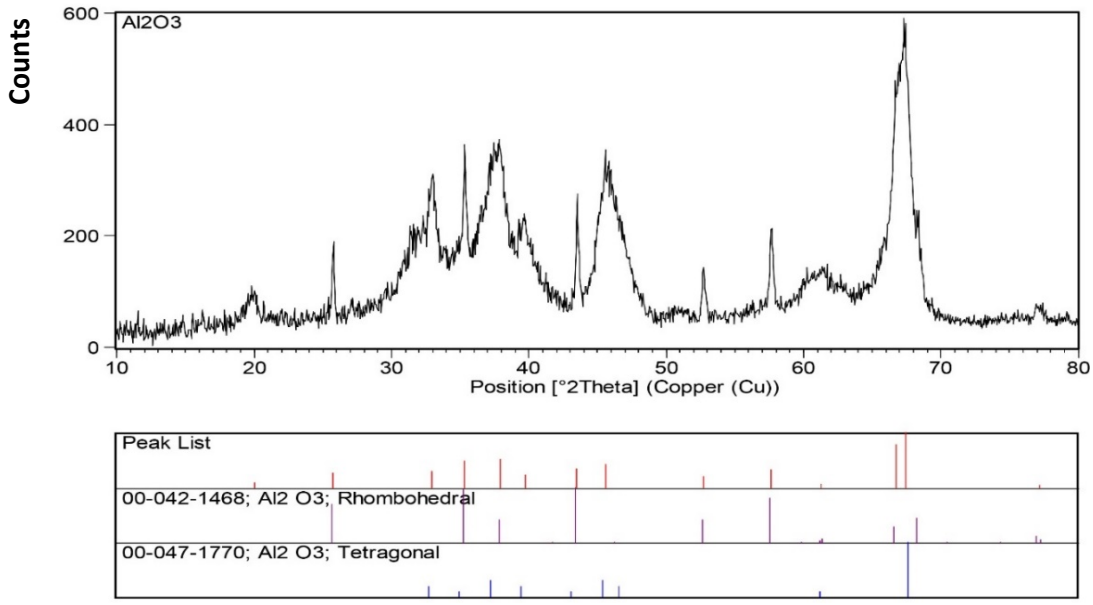

Fig. 3. XRD pattern of Al_2O_3 nanoparticles

Table 1. Average crystallite size of the samples

Sample	d (nm)
$CuFe_2O_4$	35
Al_2O_3	45

1770.

The crystallite size of samples was calculated from the full width at half maximum (FWHM) of the diffraction peaks using Debye-Scherrer's equation:

$$d=\frac{k\lambda}{\beta\cos\theta} \quad (1)$$

where d is the average crystalline dimension perpendicular to the reflecting phases, λ is the x-ray wavelength, k is Scherrer constant (0.94), β is the FWHM intensity of a Bragg reflection excluding instrumental broadening and θ is the Bragg angle [27,28]. Table 1 indicates the calculated average crystallite size of the both samples.

Fig. 4(a,b) show the SEM image of copper ferrite synthesized by hydrothermal method and hydrothermal method assisted by ultrasound waves. As it can be seen in Fig. 4-a, the nanostructure consists of small and uniform grains with average diameter of 42 nm that are stuck together in some areas. The small size of these particles is very important to optimize their magnetic properties. Hydrothermal method is a simple method to obtain nanoparticles with ideal size, but SEM images of copper ferrite synthesized by ultrasonic method (Fig. 4-b) shows smaller and more uniform nanoparticles without agglomeration. By applying ultra-sound waves with trapping air in the solvent, nano bubbles are created in the solvent, as we know after collapsing and exploding of bubbles micro jet are created that can prepare high energy for breaking of bonds and agglomeration. As a results mono-disperse nanoparticles with average size around 30 nm were prepared.

Fig. 5(a,b) discloses SEM images of alumina prepared by hydrothermal method at 250°C and hydrothermal method assisted by ultrasound waves (400 W, 60 min). As it can be seen, compared to Fig. 5-a, the structure of alumina synthesized by ultrasonic method (Fig. 5-b) is very uniform and contains small grains with average size of 48 nm. The porous structure in Fig. 5-b indicates the readiness of a suitable nanostructure of alumina

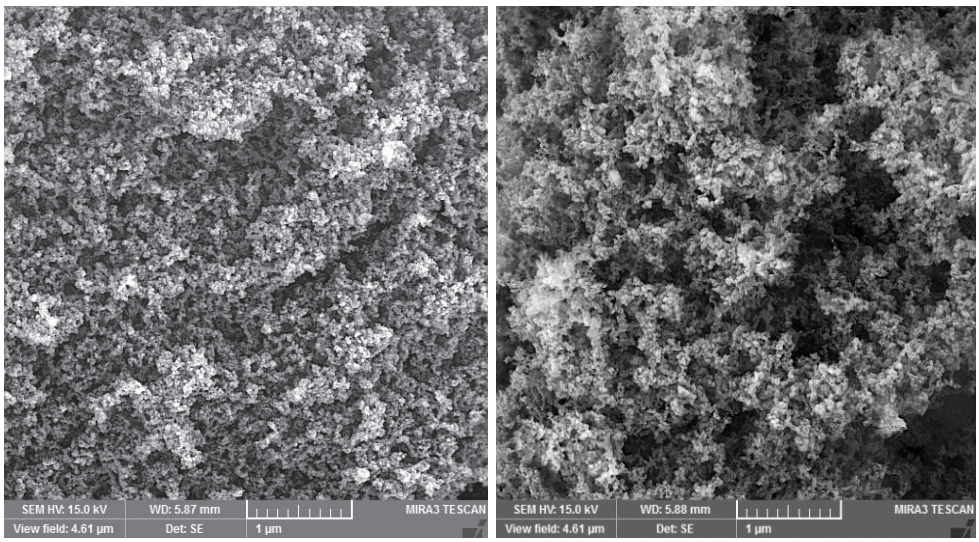

(a) **(b)**

Fig. 4. SEM images of copper ferrite synthesized by: a) hydrothermal method b) hydrothermal method assisted by ultrasound waves

for photocatalytic behavior. Fig. 6 illustrates SEM images of $Al_2O_3/CuFe_2O_4$ nanocomposite. Despite the combination of two different materials, one of which is a magnetic material and the other is a strong absorber, fortunately, uniform and very small size nanoparticles without any agglomeration in a porous structure are seen in this figure. The average size of nanoparticles was achieved 59 nm by SEM. Obtaining nanoparticles with uniform structure and suitable size using a simple chemical method and especially without the presence of surfactant and expensive

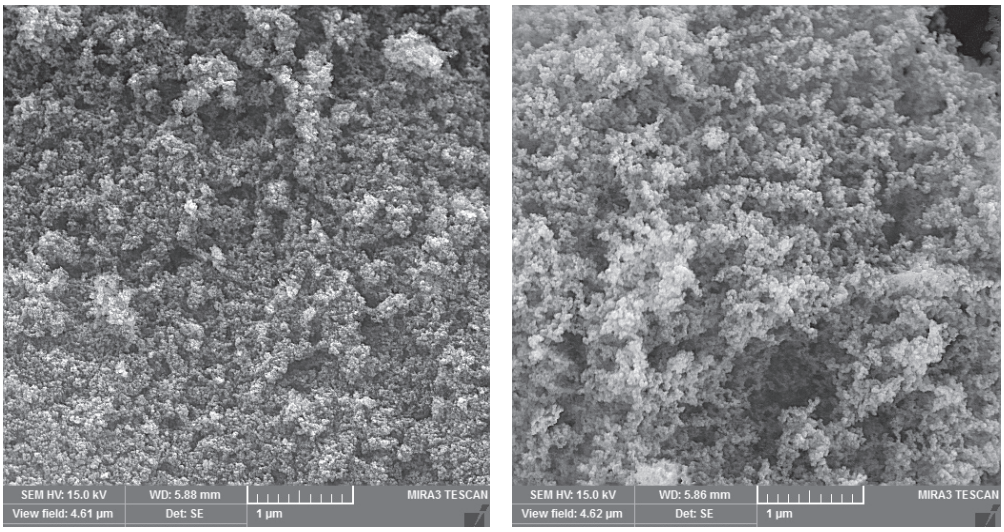

(a) **(b)**

Fig. 5. SEM images of alumina synthesized by: a) hydrothermal method b) hydrothermal method assisted by ultrasound waves

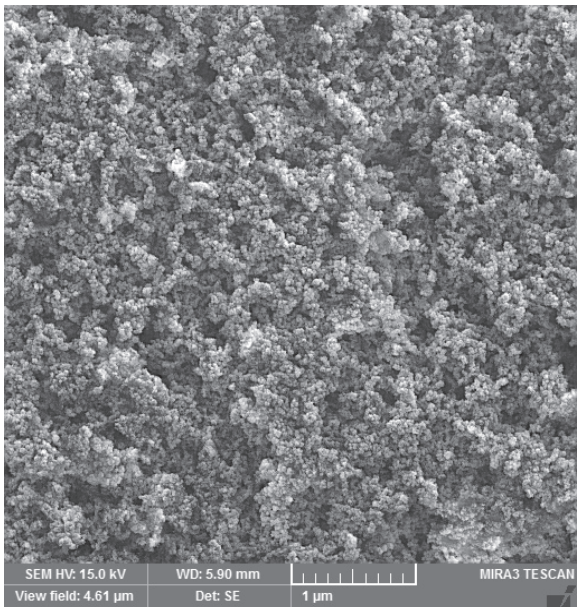

Fig. 6. SEM image of $Al_2O_3/CuFe_2O_4$ nanocomposite

equipment, is a difficult task which has been made possible in this synthesis.

Fig. 7 reveals the average particle diameters for all synthesized samples that compared through a bar chart.

Magnetic properties of $CuFe_2O_4$ and our nanocomposite were studied by VSM instrument at room temperature. Fig. 8(a,b) shows the hysteresis loops of these samples. The shape of curves and the low values of residual magnetization and coercivity indicates that both samples have superparamagnetic properties. Also Table 2 shows magnetic parameters related to these two samples.

Photocatalytic activity of Al_2O_3 /$CuFe_2O_4$ nanocomposite

The photocatalytic activity of Al_2O_3 /$CuFe_2O_4$ nanocomposite were investigated in this work.

Active radicals that generated by Al_2O_3 react with organic pollutants, deleted them and produce CO_2 and H_2O.

Alumina with E_g= 3.7 eV is activated with UV light. The electrons are excited by absorbing UV light from valence band to conduction band. The electron- hole pairs are able to reduce and/or oxidize a molecule adsorbed (O_2, H_2O and etc.) on the photocatalyst semiconductor surface and produce hydroxyl radicals (OH^-) and superoxide

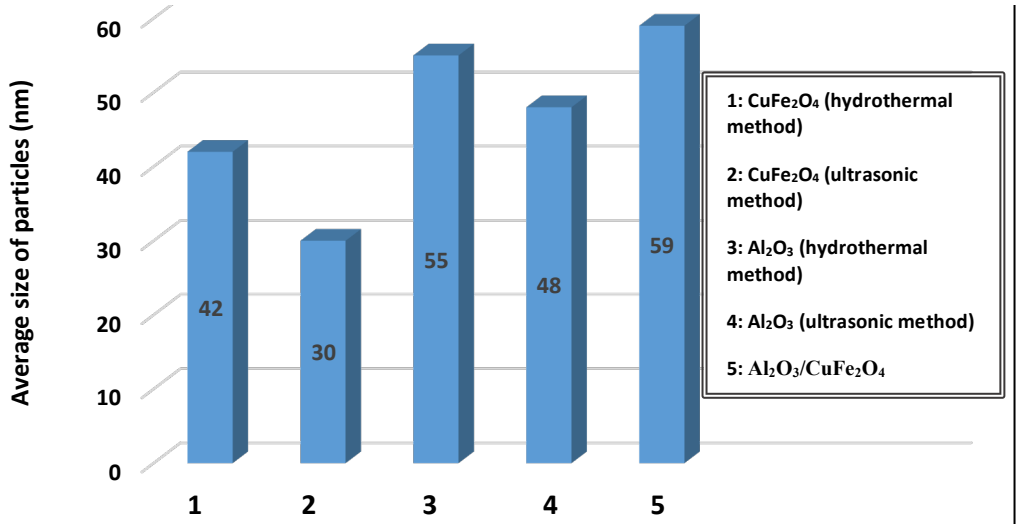

Fig. 7. The average grain diameters for all synthesized samples

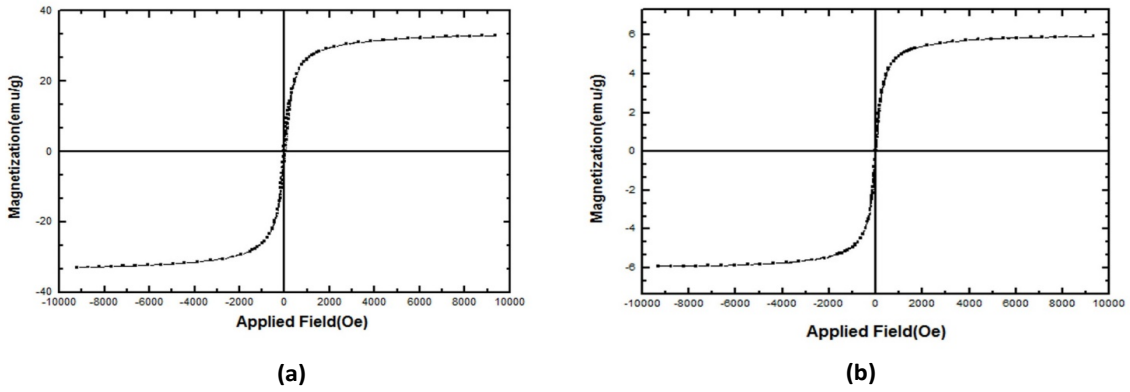

Fig. 8. Hysteresis loops for: a) $CuFe_2O_4$ b) Al_2O_3/$CuFe_2O_4$ nanocomposite

Table 2. Magnetic parameters of $CuFe_2O_4$ nanoparticles and Al_2O_3/$CuFe_2O_4$ nanocomposite

Sample	Saturation magnetization M_s (emu/g)	Residual magnetization M_r (emu/g)	Coercivity (Oe)	$\frac{M_r}{M_s}$
$CuFe_2O_4$	32	4.2	80	0.131
$CuFe_2O_4/Al_2O_3$	5.9	0.8	50	0.135

anion radicals ($O_2^{\cdot-}$). Following reactions are happened during degradation of pollutants on the Al_2O_3 surface:

$$Al_2O_3 + h\nu\ (\text{UV light}) \rightarrow e^- + h^+ \quad (2)$$

$$H_2O + h^+ \rightarrow OH^\cdot + H^+ \quad (3)$$

$$O_2 + 2e^- + 2H^+ \rightarrow H_2O_2 \quad (4)$$

$$H_2O_2 + e^- + H^+ \rightarrow OH^\cdot + H_2O \quad (5)$$

$$2H_2O + 2h^+ \rightarrow 2H^+ + H_2O_2 \quad (6)$$

Addition of copper ferrite to Al_2O_3 and preparation of Al_2O_3 /$CuFe_2O_4$ nanocomposite, in addition to helping to remove photocatalytic reaction products from the aqueous medium by applying an external magnetic field, also helps to improve the photocatalytic properties of alumina. The energy gap of copper ferrite is about 1.42 eV in the region of visible light energy.

In Al_2O_3 /$CuFe_2O_4$ nanocomposite, the transfer of holes and electrons occurs in the energy bands of both materials (Increasing charge carriers and as a result, increase the photocatalytic reactions). It is expressive of reduced recombination of charge carriers, leading to availability of more reactive radicals in nanocomposite for the enhanced photocatalytic activity. Superoxide anion radicals generated by $CuFe_2O_4$ can react with hydrogen peroxide and leading to hydroxyl radical's production [29, 30]:

$$H_2O_2 + O_2^{\cdot-} \rightarrow OH^\cdot + OH^- + O_2 \quad (7)$$

Fig. 9 shows the coupling mechanism of two materials for photocatalytic activity.

To analyze the photocatalytic behavior of prepared nanocomposites, we used methyl orange ($S_3NaO_3N_{14}H_{14}C$) and methyl red ($C_{15}H_{15}N_3O_2$) as natural contaminant. These dyes are widely used in photocatalytic researches due to their structural stability.

First, using distilled water as solvent, color solutions were prepared with two concentrations of 50ppm and 100ppm of these two dyes, and by adding hydrochloric acid, acidic dye solutions

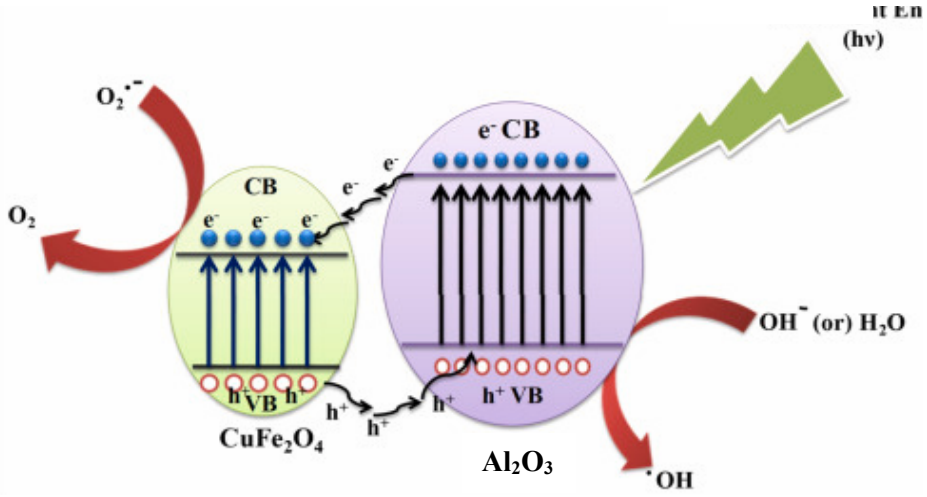

Fig. 9. Schematic of photo-catalyst levels under solar irradiation

with a pH of 4 were obtained. Then the absorption spectra of these solutions under UV-visible radiation in the wavelength range of 250- 700nm were obtained by UV-visible spectrometer and the maximum absorption wavelength (λ_{max}) was determined for each dye solution.

Then in 20ml of dye solutions with concentrations of 50ppm and 100ppm, 0.1g of nanocomposite was added as adsorbent. After resting in a dark place for a few hours, the dye solutions were stirred with a magnetic stirrer. They were exposed to UV-visible radiation for 30 minutes. This experiment was repeated for 60 and 90 min. irradiation time with the same conditions.

Fig. 10 schematically shows the mechanism of dye degradation under irradiaton.

At the end of the irradiation time for each of the dye solutions, the final absorbance at λ_{max} was determined by the spectrometer and using these results, the percentage of reduction of the dye concentration (degradation efficiency) was obtained from the following equation in each experiment:

$$\eta = \frac{Co - Cf}{Co} \times 100 \quad (8)$$

Where C_0 and C_f are the initial and final azo dye

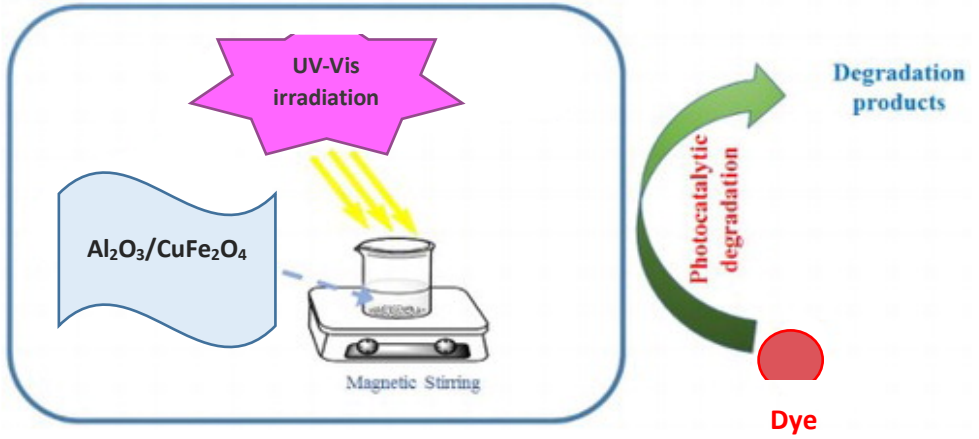

Fig. 10. Mechanism of dye degradation

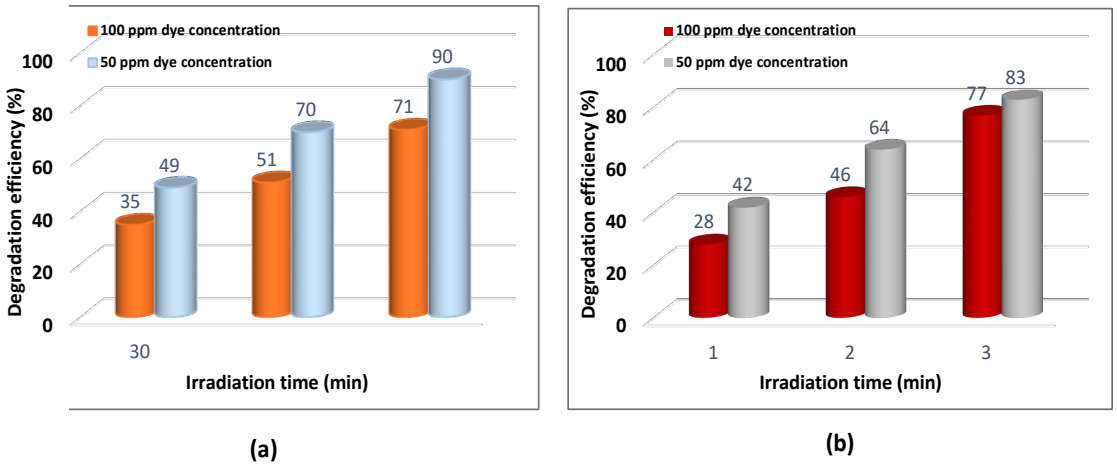

Fig. 11. The results of degradation efficiency for dye solutions with two different dye concentrations at different irradiation times: a) methyl orange b) methyl red

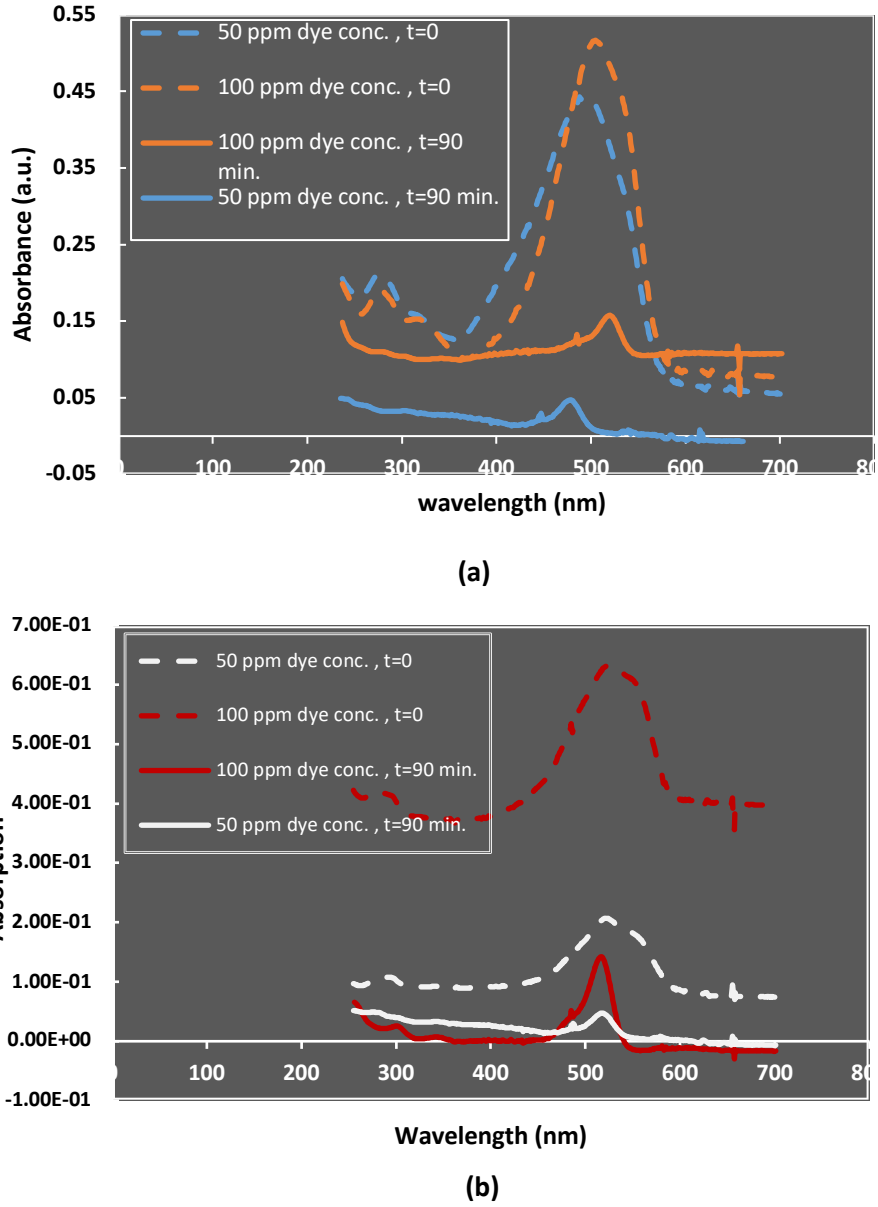

Fig. 12. The effect of $Al_2O_3/CuFe_2O_4$ nanocomposite on degradation of dye solutions with different dye concentration: a) methyl orange b) methyl red

concentrations respectively.

Fig. 11(a,b) visualize the results of degradation efficiency for two dye solutions in 50 and 100 ppm dye concentrations at different irradiation times. Degradation efficiency increases with the irradiation time. Because with prolongation of irradiation time, the amount of reactive free radicals will increase. As the concentration of dye solution increases from 50ppm to 100ppm, the degradation efficiency decreases. The reason being the number of reactive free radicals for degradation of dyes being the same in each concentration, but the amount of pollutants (the dyes) increasing.

Fig. 12(a,b) illustrates the changes in the dye concentration by adding 0.1 g of Al_2O_3 /$CuFe_2O_4$

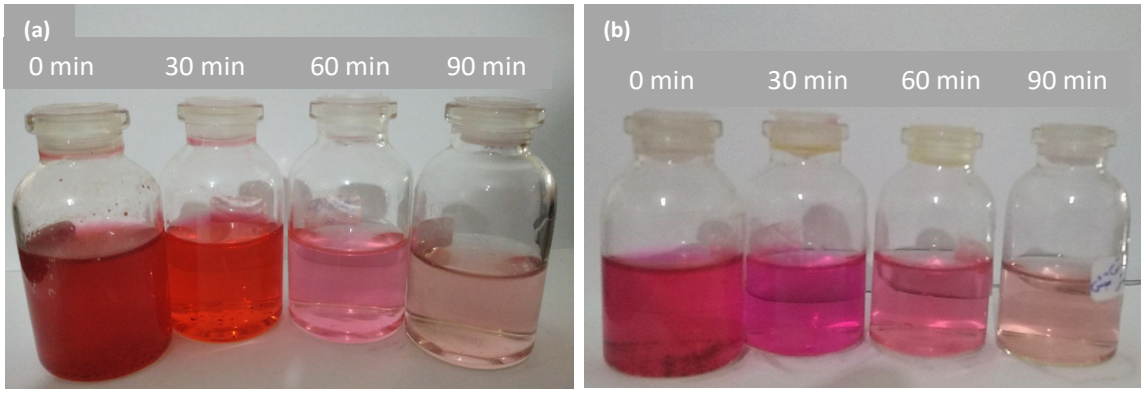

Fig .13. Photo degradation of 20 ml of azo dyes solutions with 0.1 g adsorbent and 50 ppm dye concentration under 0, 30, 60 and 90 min solar irradiation: a) methyl orange b) methyl red

nanocomposite to two different dye solutions with 50 and 100ppm concentration of dye after 90 minutes irradiation from UV-vis absorption spectra. Also Fig. 13(a,b) shows the color degradation of these dye solutions during the irradiation time.

CONCLUSION

In the first step, $CuFe_2O_4$ and Al_2O_3 nanoparticles were synthesized by hydrothermal method. The synthesis was repeated once in the presence of ultrasound waves to determine the effect of these waves on improving the nanostructure and grain size of the samples.

Then Al_2O_3 /$CuFe_2O_4$ nanocomposite was prepared by the same method. The hysteresis curves obtained using the VSM analysis showed that both of $CuFe_2O_4$ and Al_2O_3 /$CuFe_2O_4$ had superparamagnetic properties.

Finally, the photocatalytic behavior of Al_2O_3 / $CuFe_2O_4$ nanocomposite was studied using the degradation of methyl orange and methyl red solutions with two dye concentration under different times of UV-visible light irradiation. The nanocomposite had the photocatalytic properties. The color degradation increased with increasing the irradiation time until the degradation efficiency reached 77% for 100ppm and 83% for 50ppm dye concentrations of methyl red solution and 71% and 90% for same conditions of methyl orange solution after 90 minutes irradiation respectively.

CONFLICT OF INTEREST

The authors declare that there is no conflict of interests regarding the publication of this manuscript.

REFERENCES

1. Jiles D. Magnetic Materials. Introduction to Magnetism and Magnetic Materials: CRC Press; 2015. p. 83-106.
2. Roy D, Shivakumara C, Anil Kumar PS. Observation of the exchange spring behavior in hard–soft-ferrite nanocomposite. Journal of Magnetism and Magnetic Materials. 2009;321(5):L11-L14.
3. Tanaka T, Matsuzaki J, Kurisu H, Yamamoto S. Magnetization behavior of hard/soft-magnetic composite pillar. Journal of Magnetism and Magnetic Materials. 2008;320(22):3100-3103.
4. Lu AH, Salabas EL, Schüth F. Magnetic Nanoparticles: Synthesis, Protection, Functionalization, and Application. Angew Chem Int Ed. 2007;46(8):1222-1244.
5. Merikhi M, Nabiyouni G, Ghanbari B. Effect of magnetic field on surface morphology and magnetic properties of FeCu/Cu nano layers prepared by electrodeposition technique: investigation of magneto-hydrodynamic effect. Journal of Nanostructures.2015; 5: 409-414.
6. Singh S, Yadav BC, Gupta VD, Dwivedi PK. Investigation on effects of surface morphologies on response of LPG sensor based on nanostructured copper ferrite system. Materials Research Bulletin. 2012;47(11):3538-3547.
7. Iqbal MJ, Yaqub N, Sepiol B, Ismail B. A study of the influence of crystallite size on the electrical and magnetic properties of $CuFe_2O_4$. Materials Research Bulletin. 2011;46(11):1837-1842.
8. Zakiyah LB, Saion E, Al-Hada NM, Gharibshahi E, Salem A, Soltani N, Gene S. Up-scalable synthesis of size-controlled copper ferrite nanocrystals by thermal treatment method. Mater Sci Semicond Process. 2015;40:564-569.
9. Nabiyouni GH, Ghanbari D. Hydrothermal synthesis of magnetic and photoluminescence $CuFe_2O_4$-carbon dots nanocomposite as a sensor for detecting of Hg(Π) ions. Journal of Nanostructures. 2020; 10: 760-768.
10. Clark JB, Hastie JW, Kihlborg LHE, Metselaar R, Thackeray MM. Decomposition V Gold, K L Loening, A D McNaught and P Sehmi, in Compendium of Chemical Technology: IUPAC Recommendations (The IUPAC "Gold Book"), Blackwell Scientific Publications, Oxford, 1987. IUPAC Standards Online: De Gruyter; 2016.

11. Bai JZ, Ban Y, Bian JG, Blum I, Chen AD, Chen GP, et al. Radiative decay of the ψ (2S) into two pseudoscalar mesons. PhRvD. 2003;67(3).
12. Kanhere P, Chen Z. A Review on Visible Light Active Perovskite-Based Photocatalysts. Molecules. 2014;19(12):19995-20022.
13. Parsons S. Advanced Oxidation Processes for Water and Wastewater Treatment. Water Intelligence Online. 2015;4(0):9781780403076-9781780403076.
14. Yin L, Wang D, Huang J, Cao L, Ouyang H, Yong X. Morphology-controllable synthesis and enhanced photocatalytic activity of ZnS nanoparticles. Journal of Alloys and Compounds. 2016;664:476-480.
15. Muruganandham M, Amutha R, Repo E, Sillanpää M, Kusumoto Y, Abdulla-Al-Mamun M. Controlled mesoporous self-assembly of ZnS microsphere for photocatalytic degradation of Methyl Orange dye. J Photochem Photobiol A: Chem. 2010;216(2-3):133-141.
16. Mohamed RM, McKinney DL, Sigmund WM. Enhanced nanocatalysts. Materials Science and Engineering: R: Reports. 2012;73(1):1-13.
17. Ghanbari D. Green synthesis of $C@Fe_3O_4@Ag$ nanocomposites: coating of silver nanoparticles on the carbon template/magnetite as a catalyst for conversion of toxic carbon monoxide to carbon dioxide. Journal of Nanostructures. 2021; 11: 297-304.
18. Soltani N, Saion E, Yunus WMM, Erfani M, Navasery M, Bahmanrokh G, Rezaee K. Enhancement of visible light photocatalytic activity of ZnS and CdS nanoparticles based on organic and inorganic coating. Applied Surface Science. 2014;290:440-447.
19. Zhang Y, Wu B, Xu H, Liu H, Wang M, He Y, Pan B. Nanomaterials-enabled water and wastewater treatment. NanoImpact. 2016;3-4:22-39.
20. Faungnawakij K, Kikuchi R, Shimoda N, Fukunaga T, Eguchi K. Effect of Thermal Treatment on Activity and Durability of $CuFe_2O_4$–Al_2O_3 Composite Catalysts for Steam Reforming of Dimethyl Ether. Angew Chem Int Ed. 2008;47(48):9314-9317.
21. Wu X, Song X, Chen H, Yu J. Treatment of phenolic compound wastewater using $CuFe_2O_4$–Al_2O_3 particle electrodes in a three-dimensional electrochemical oxidation system. Environ Technol. 2020;42(28):4393-4404.
22. Subramanian V, Gnanakumar ES, Jeong D-W, Han W-B, Gopinath CS, Roh H-S. A rationally designed $CuFe_2O_4$–mesoporous Al_2O_3 composite towards stable performance of high temperature water–gas shift reaction. Chemical Communications. 2013;49(96):11257.
23. Nabiyouni GH, Ahmadyand N, Najafi M, Ghanbari D. Growth and characterization of iron nanowires into anodized aluminum oxide templates using electrodeposition technique. Journal of Nanostructures. 2019; 9: 437-441.
24. Yadav SK, Jeevanandam P. Synthesis of PbS– Al_2O_3 nanocomposites by sol–gel process and studies on their optical properties. Optical Materials. 2015;46:209-215.
25. Behzadi M, Jarollahi S, Ahsani Irvani M, Ghanbari D. Green synthesis and antibacterial activity of silver nanoparticles using dracocephalum moldavica leaves extract. Journal of Nanostructures. 2022; 12(4): 1059-1066.
26. Amini R, Nabiyouni G, Jarollahi S. Removal of azo dyes pollutants: photo catalyst and magnetic investigation of iron oxide-zinc sulfide nanocomposites. Journal of Nanostructures. 2021; 11(1): 95-104.
27. Manohara BM, Nagabhushana H, Thyagarajan K, Prasad BD, Prashantha SC, Sharma SC, Nagabhushana BM. Synthesis and Photoluminescence Properties of $CdSiO_3$:Ho^{3+} Nanophosphor. Advanced Science Letters. 2016;22(4):785-789.
28. Nowick AS. X-ray diffraction procedures for polycrystalline and amorphous materials. H. P. Klug and L. E. Alexander. John Wiley and Sons, Inc., New York (1954). 716 pages. $15.00. AIChE Journal. 1956;2(1):140-140.
29. Abdi Z, Maghazeii F, Ghanbari D. The Effect of Calcium Perovskite and Newly Developed Magnetic $CaFe_2O_4$/$CaTiO_3$ Perovskite Nanocomposite on Degradation of Toxic Dyes Under UV–Visible Radiation. Journal of Cluster Science. 2021;33(6):2475-2487.
30. Kiani A, Nabiyouni G, Masoumi S, Ghanbari D. A novel magnetic $MgFe_2O_4$–$MgTiO_3$ perovskite nanocomposite: Rapid photo-degradation of toxic dyes under visible irradiation. Composites Part B: Engineering. 2019;175:107080.